Entanglement patterns and pure quantum correlations in the Heisenberg *XY* model

F. B. M. dos Santos, R. M. Dias, and A. M. S. Macêdo
Departamento de Física, Laboratório de Física Teórica e Computacional, Universidade Federal de Pernambuco, 50670-901 Recife, Pernambuco, Brazil

(Received 25 August 2008; revised manuscript received 19 January 2009; published 24 March 2009)

We investigate the possibility of the existence of different types of thermal entanglement in the two-spin Heisenberg *XY* model, which are distinguished by the behavior of the concurrence as a function of the model parameters. Singularities in the temperature threshold for thermal entanglement and in the ground-state energy as a function of the model parameters are used to construct diagrams containing boundary lines separating the several types of thermal entanglement in the system, showing an unexpected rich structure. We discuss a procedure to extract a pure quantum component from the spin-correlation function at arbitrary temperatures, by using the explicit form of the decomposition that minimizes the concurrence, and show that it is highly sensitive to the different patterns of thermal entanglement.

DOI: 10.1103/PhysRevA.79.032329 PACS number(s): 03.67.Mn, 03.65.Ud, 75.10.Jm

I. INTRODUCTION

Entanglement is a fundamental quantum-mechanical feature which sets the basic differences between classical and quantum correlations. It is regarded as a valuable resource in quantum information processing [1,2] and has been the subject of intense research over the last few years [3]. The study of entanglement in condensed-matter systems is more recent and is expected to provide insights in the description of many-body quantum effects, such as quantum magnetism, superconductivity, quantum Hall effect, and quantum phase transitions [4]. These expectations have motivated efforts [5,6] to analyze the properties of entanglement in many-body systems and to identify the possible consequences of these properties in physical observables. The surprising result of these studies is the conclusion that entanglement can be sustained under macroscopic thermodynamic conditions in condensed-matter systems [7].

Most of the works on entanglement in condensed-matter systems addressed the problem of its quantification as a function of some controlled parameters. In the case of pure states in bipartite systems, the degree of entanglement can be measured by the von Neumann entropy [8], which is calculated from the reduced density matrix obtained by performing a partial trace of the total density matrix over one of the subsystems. Using this measure it became possible to study many properties of entanglement in the ground state of several many-body systems [5,6]. The quantification of entanglement in mixed states, however, is more complicated because the measures of entanglement do not lead to direct computational schemes for arbitrary mixed states. The entanglement of formation [8], for example, yields a closed exact solution only in the simplest case of two qubits [9]. For an arbitrary number of qubits, it has so far only been possible to estimate upper and lower bounds to the entanglement of formation [10], in which case the concept of negativity [11] is also important. Such state of affairs has made it difficult to study more systematically the properties of entanglement in more realistic many-body systems such as those in contact with a thermal bath and/or in the presence of quantum noise.

Particularly important many-body systems, whose entanglement properties have attracted much attention of the condensed-matter community, are chains of quantum spins. The possibility to map quantum walks [12], whose theory may provide a powerful way to systematize quantum algorithms, onto networks of quantum spins [13] is one of the motivations to study these systems in the context of quantum computing and quantum information. A particularly attractive feature of quantum spin chains is the possibility of finding exact expressions of entanglement quantifiers for certain types of interactions. For instance, the von Neumann entropy which quantifies entanglement in the ground state of the Heisenberg *XY* spin chain has an exact expression in the thermodynamic limit [14–16]. Other models of quantum spin chains have recently been studied using methods from random-matrix theory [17].

The thermal pairwise entanglement between two arbitrary spins in the Heisenberg *XY* model has been extensively studied. In the case of the two-spin chain, many exact solutions are available [18–21]. For chains with more than two spins, the pairwise entanglement between any two spins can be calculated by using the reduced density matrix obtained by performing the partial trace over all the remaining spins of the chain [22–25]. In both cases, the most striking feature is the vanishing of the entanglement for temperatures above a certain finite threshold T_c. This is argued to be a general property of entanglement in bipartite systems in contact with a thermal bath [26]. The existence of a temperature interval, below the critical temperature, on which the entanglement of formation vanishes has also been recently reported [19,25].

An important feature of ground-state entanglement is its role as an indicator of a quantum phase transition [4]. The derivative of the concurrence with respect to the parameter driving the transition has been shown to exhibit well-defined scaling properties [5,6,22,27]. Another interesting prospect is the possibility that entanglement be used as a generalized concept of order [7], which could not only unify currently widely accepted definitions of order via correlation function but also give rise to new kinds of orders in condensed-matter systems, such as the topological/quantum orders introduced by Wen [28]. The basic idea can be summarized as follows. The concept of order in condensed-matter systems is intrinsically connected to the existence of certain types of correlations between different parts of the system. The notion of

symmetry breaking provides in Landau's theory a classification of the possible orders and also determines the general structure of the low-energy effective description in terms of the Nambu-Goldstone modes. Quantum orders appear naturally in fractionally quantum Hall systems and are different in that they cannot be described by Landau's theory. They result from new kinds of nonlocal quantum correlations that sustain an ordered pattern without breaking any symmetry. In Ref. [29] quantum orders were associated with different patterns of quantum entanglement. This interesting connection allowed an understanding of some unusual features of entanglement through the study of the ground state of exact soluble models and also provided a classification of entanglement patterns associated with quantum orders in terms of projective symmetry groups [28,29].

Being a generic property of the density matrix of a quantum state, we should expect entanglement patterns to also emerge in thermal states of finite systems, although the concept of quantum order itself, defined via singularities in the energy density, does not rigorously apply to finite systems, which would imply a conceptual difference between entanglement patterns in finite systems and quantum order. Considering the current technological limitations in scaling the number of entangled qubits in artificially constructed devices, the possibility to distinguish between different types of entanglement in qubit clusters is quite appealing from a conceptual point of view. Interesting practical questions could arise, such as the possibility to induce a certain entanglement pattern in a given set of qubits, a situation that is conceptually similar to the phenomenon of spin injection in spintronics [30].

In this paper, we investigate the possibility of distinguishing entanglement patterns in finite systems through the study of the thermal entanglement in the two-spin Heisenberg *XY* chain. We propose to use the behavior of the concurrence as a function of the model parameters as a classifier of entanglement patterns. Our results are presented in diagrams, whose boundary lines are related to singularities in the ground-state energy and in the temperature threshold for thermal entanglement as a function of the model parameters. We have used Wootters' concurrence minimization procedure to extract a pure quantum component from the spin-correlation functions. We show that this pure quantum component is highly sensitive to changes in the patterns of thermal entanglement as one crosses the boundary lines of the diagrams. The paper is organized as follows. In Sec. II, we present a brief description of the thermal entanglement of the system by means of Wootters' formula for the concurrence [9]. We calculate the entanglement threshold T_c and show that it agrees with previous results [18,21]. We also observe the existence of a temperature interval below T_c, denoted *entanglement dip*, where the entanglement vanishes [19,25]. In Sec. III we provide a characterization of possible entanglement patterns in the model by using the concurrence as a function of the model parameters. The results are presented via diagrams whose boundary lines separate regions with different types of entanglement. These diagrams introduce concepts which extend in a nontrivial way previous analysis of the two-spin Heisenberg *XY* model, where the concurrence was used simply as a tool to distinguish entangled from separable mixed states. In Sec. IV, we derive the concurrence-minimizing or optimal decomposition, and using it, we propose a procedure to extract a pure quantum component from the spin-correlation functions at finite temperature. We show that many properties of the thermal entanglement, such as the emergence of a temperature threshold and the existence of entanglement dips, appear as notable features in the pure quantum spin-correlation functions. Such signatures are lost, however, when the ensemble average is performed. A summary and conclusions are presented in Sec. IV.

II. GENERAL PROPERTIES OF THE THERMAL ENTANGLEMENT

The Hamiltonian of the Heisenberg *XY* model describing two spins in the presence of a uniform magnetic field h applied in the z direction can be written as $H=hH_\alpha$, where H_α is given by

$$H_\alpha = -\frac{\alpha}{2}[(1+\gamma)\sigma_1^x\sigma_2^x + (1-\gamma)\sigma_1^y\sigma_2^y] - (\sigma_1^z + \sigma_2^z), \quad (1)$$

where the anisotropy parameter γ ranges from $\gamma=0$ (XX model) to $\gamma=1$ (Ising model), $\alpha=J/h$ where J is the coupling constant, and σ_j^k corresponds to the Pauli operator in the direction $k\in\{x,y,z\}$ for the jth spin.

We assume that the system is in contact with a thermal bath [23] with inverse temperature parameter β. We verify that the transition from entangled to separable state occurs as expected at a finite temperature T_c [18,21–23], which we shall present as a function of the model parameters. We also observe the appearance of dips of vanishing concurrence, denominated entanglement dips, which occur on a temperature interval below T_c, in agreement with recent works [19,25].

When the system is in contact with a thermal bath, the resulting mixed state is described by the density matrix $\rho = Z^{-1}\exp(-H_\alpha/T)$, where Z is the partition function and $T \equiv (h\beta)^{-1}$. From the matrix representation of H in the base $\{|00\rangle,|01\rangle,|10\rangle,|11\rangle\}$ we find

$$\rho = \frac{1}{Z}\begin{pmatrix} p & 0 & 0 & q \\ 0 & \cosh\Delta & \sinh\Delta & 0 \\ 0 & \sinh\Delta & \cosh\Delta & 0 \\ q & 0 & 0 & r \end{pmatrix}, \quad (2)$$

where

$$p = \cosh\Delta_c + \frac{2}{\sqrt{4+\alpha^2\gamma^2}}\sinh\Delta_c,$$

$$q = \frac{\alpha\gamma}{\sqrt{4+\alpha^2\gamma^2}}\sinh\Delta_c,$$

$$r = \cosh\Delta_c - \frac{2}{\sqrt{4+\alpha^2\gamma^2}}\sinh\Delta_c,$$

$$Z = 2(\cosh\Delta + \cosh\Delta_c),$$

$$\Delta = \alpha/T,$$

$$\Delta_c = \sqrt{4+\alpha^2\gamma^2}/T.$$

The concurrence of the system in this state can be calculated using Wooters' formula [9] for the convex roof of the concurrence. In order to apply this procedure we need to calculate the square root of the eigenvalues of the non-Hermitian matrix $R \equiv \rho\tilde{\rho} = \rho\sigma^y \otimes \sigma^y \rho^* \sigma^y \otimes \sigma^y$. We obtain four different values,

$$\lambda_1 = \frac{\sqrt{1+q^2}-q}{Z}, \tag{3}$$

$$\lambda_2 = \frac{\sqrt{1+q^2}+q}{Z}, \tag{4}$$

$$\lambda_3 = \frac{e^{-\Delta}}{Z}, \tag{5}$$

$$\lambda_4 = \frac{e^{+\Delta}}{Z}. \tag{6}$$

We shall consider, without loss of generality, just the case in which α and h are positive. The maximum eigenvalue can then be either λ_2 or λ_4 and thus there are two possible expressions for nonzero values of the concurrence, $C_2(\rho)=\lambda_2-\lambda_1-\lambda_3-\lambda_4$ and $C_4(\rho)=\lambda_4-\lambda_1-\lambda_2-\lambda_3$. The concurrence can therefore be written as $C(\rho)=\max\{0, C_2(\rho), C_4(\rho)\}$, where

$$C_2(\rho) = \frac{2}{Z}[q - \cosh\Delta], \tag{7}$$

$$C_4(\rho) = \frac{2}{Z}[\sinh\Delta - \sqrt{1+q^2}]. \tag{8}$$

Due to parity symmetry the density matrix decomposes into two blocks, denoted parallel and antiparallel. The eigenvalues λ_1 and λ_2 are obtained from the parallel block while λ_3 and λ_4 arise from the antiparallel one. This distinction is useful in the interpretation of the functions C_2 and C_4 as parallel and antiparallel entanglement measures [31,32]. These two types of entanglement are usually interpreted as being derived from different spin configurations which can be described in terms of the probabilities of the occurrence of parallel or antiparallel Bell states. The interpretation in terms of probabilities works very well for the ground state (pure state), but for the thermal state it leads to some difficulties as was recently reported in Ref. [32]. In Sec. III, we will show that the concurrences C_2 and C_4 are obtained from different families of concurrence-minimizing decompositions, which in turn explains the differences in their behavior.

In Fig. 1 we show three-dimensional graphs $C \times \alpha \times \gamma$ for different temperatures. At low temperatures, the behavior of the concurrence is strongly affected by its value in the ground state. There are two regimes separated by a curve $\alpha_c(\gamma)$ where the ground-state concurrence presents a discontinuity, which is related to an abrupt change in the ground state itself. For finite temperature, on the other hand, the discontinuity at $\alpha=\alpha_c$ gives rise to the steep decline shown in Fig. 1(a). Increasing the temperature further, the transition between the two regimes becomes smoother [Fig. 1(b)] and the concurrence begins to vanish, initially in the region $\alpha < \alpha_c$ [Fig. 1(c)] and then, above a certain threshold, it vanishes everywhere. In fact, for an arbitrary pair of parameter values (α, γ), one can always find a critical temperature T_c

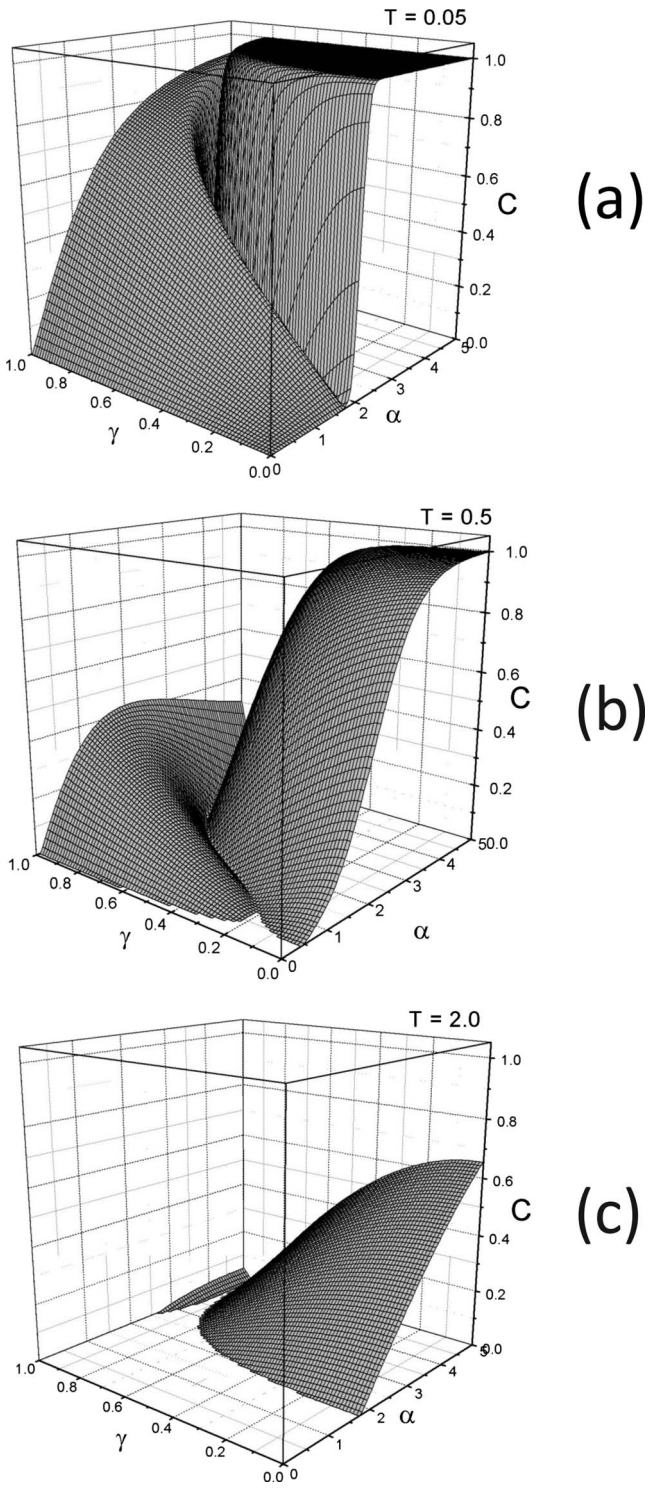

FIG. 1. Three-dimensional graphs of the concurrence as a function of the parameters α and γ for different temperatures.

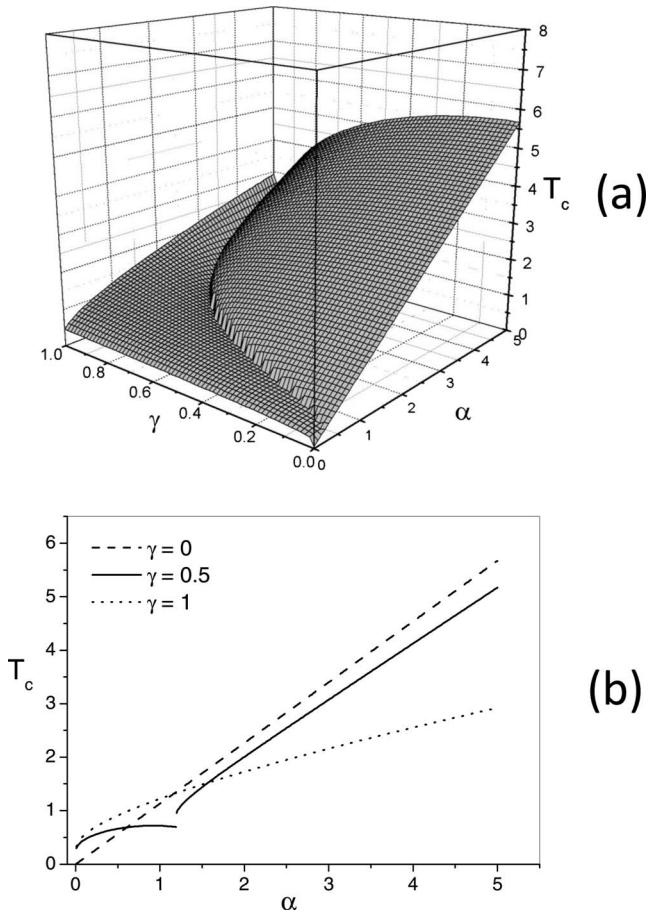

FIG. 2. (a) Three-dimensional graph of the critical temperature T_c as a function of α and γ. (b) Cross sections for several values of γ. For values of γ different from $\gamma=0$ and $\gamma=1$, there is a discontinuity in T_c as a function of α at the point α_t, which defines a curve $\alpha_t(\gamma)$. This curve is shown in the diagram of Fig. 4, where it is used as a boundary line separating different patterns of entanglement.

above which $C(\rho)=0$. There are sound mathematical arguments [26] establishing that this transition toward zero concurrence at finite temperature, reported in many works [18,19,21,23,24], is a general property of bipartite thermal entanglement.

The determination of T_c for arbitrary α and γ involves the solution of one of the following transcendental equations: $C_2(\rho)=0$ or $C_4(\rho)=0$, in the parameter space regions where $\lambda_2>\lambda_4$ or $\lambda_2<\lambda_4$, respectively. Except for the case $\gamma=0$ and $\alpha=\alpha_c$, where we find

$$T_c=\frac{\alpha}{\ln(1+\sqrt{2})} \quad \text{for} \quad \gamma=0 \tag{9}$$

and

$$T_c=\frac{\alpha}{\operatorname{arcsinh}(\alpha/2)} \quad \text{for} \quad \alpha=\alpha_c=\frac{2}{\sqrt{1-\gamma^2}}, \tag{10}$$

it is not possible in general to obtain closed analytic expression for T_c.

Figure 2(a) shows a three-dimensional graph of $T_c(\alpha,\gamma)$ and Fig. 2(b) shows cross sections for several values of γ. Two different regimes appear, which are separated by a discontinuity located at a curve $\alpha_t(\gamma)$. Note that there is no discontinuity at the extreme values $\gamma=0$ and $\gamma=1$. For $\alpha>\alpha_t$, T_c is determined by the solution of $C_4=0$, while for $\alpha<\alpha_t$, it is obtained from the solution of $C_2=0$. The discontinuity is due to the fact that there is no value of T_c at which C_2 and C_4 vanish simultaneously. This peculiar behavior of the transition temperature is one of the signatures of the existence of different entanglement patterns in the mixed state describing the system. In Sec. III we shall describe in detail how these patterns can be characterized by the concurrence.

III. DIAGRAMS OF ENTANGLEMENT PATTERNS

Diagrams used as tools to characterize properties of thermal entanglements have appeared in many previous works [19,20,25]. However, with notable exceptions [32] the boundary lines in these diagrams separate regions of positive and null concurrence only, i.e., they only distinguish entangled from separable states. This appears quite natural from the point of view of traditional phase transition once we interpret the degree of entanglement as a kind of order parameter distinguishing a correlated (entangled) phase from an uncorrelated (separable) phase. However, if we accept the possibility that entanglement may provide a characterization of order beyond the conventional viewpoint, then it should be possible to classify different entangled phases according to certain pattern formations or certain behaviors of correlation functions. In this section, we present entanglement diagrams whose boundary lines separate different types of entanglement patterns, characterized by different classes of behavior of the concurrence as a function of the system's parameters. More specifically, our procedure consists of analyzing the concurrence function $C(\alpha,\gamma,T)$ through various cuts on the three-dimensional parameter space. Interestingly, the graphs of the concurrence as a function of one parameter, maintaining the others fixed, can be grouped according to a common shape and define continuous boundary lines separating different entanglement regimes on the space of the remaining parameters. These boundary lines can be traced back to discontinuities either in the ground state of the system or in the threshold temperature T_c. This procedure nicely complements previous analysis of this model by revealing a possible underlying structure in the quantum correlations implied by the presence of entanglement.

We start by presenting in Fig. 3 the graphs of $C(\alpha,\gamma,T)$ for several values of α and for $\gamma=0.5$. The concurrence curves for $\alpha>\alpha_c\approx 2.3091$ start with $C=1$ at $T=0$ and decrease monotonically with temperature, which can be interpreted as a result of the mixture of the maximally entangled pure ground state with the other states. Exactly at $\alpha=\alpha_c$, there is a reduction in the ground-state concurrence caused by a degeneracy in the ground state that transforms it into a mixed state and defines a new entanglement pattern.

In the region $\alpha<\alpha_c$, we have two different regimes that are separated by the curve $\alpha_t(\gamma)$. For $\alpha_t<\alpha<\alpha_c$, the concurrence vanishes on a small temperature interval, denominated entanglement dip, even though $T<T_c$ [19,25]. After the dip the concurrence increases with temperature reaching a maxi-

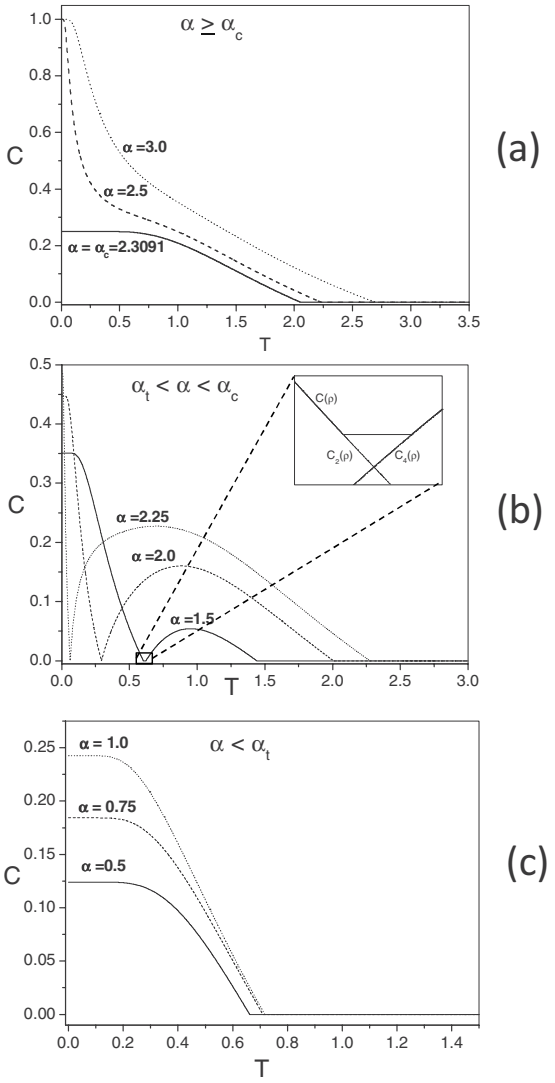

FIG. 3. Graphs of $C(\alpha,\gamma,T)$ for $\gamma=0.5$ and different values of α. Four different behaviors exist depending on the value of α: (a) monotonic decrease starting from a pure state with $C=1$ for $\alpha \geq \alpha_c=2/\sqrt{1-\gamma^2}\approx 2.3091$ and a monotonic decrease starting from mixed state for $\alpha=\alpha_c$. (b) Concurrence vanishes on a finite interval, entanglement dip (shown in the inset) for $\alpha_c \leq \alpha < \alpha_t \approx (0.193+0.648\gamma)\alpha_c \approx 1.194$. (c) Monotonic decrease starting from a pure state with $C<1$ for $\alpha<\alpha_t$.

mum value, after which it decreases monotonically until it vanishes precisely at $T=T_c$. For $\alpha<\alpha_t\approx 1.194$, we have again a simple monotonic decrease in the concurrence with temperature, but it differs from the regime where $\alpha>\alpha_c$ through the value of the ground-state concurrence.

The existence of the entanglement dip for $\alpha_t<\alpha<\alpha_c$ results from the combination of Wooters' formula [9], $C(\rho)=\max\{0,C_2(\rho),C_4(\rho)\}$, with the fact that the graphs of the functions $C_2(\rho)$ and $C_4(\rho)$ as a function of temperature never cross for $C(\rho)>0$. For $\alpha>\alpha_c$, $C(\rho)=C_4(\rho)$ defines the non-null part of the concurrence shown in Fig. 3(a), while for $\alpha<\alpha_t$, the non-null part of the concurrence is given by $C(\rho)=C_2(\rho)$. In the intermediate regime, where $\alpha_t<\alpha<\alpha_c$, both $C_2(\rho)$ and $C_4(\rho)$ contribute to $C(\rho)$ on different temperature intervals. Since their graphs do not cross for $C(\rho)>0$, there must exist a finite interval where the concurrence vanishes.

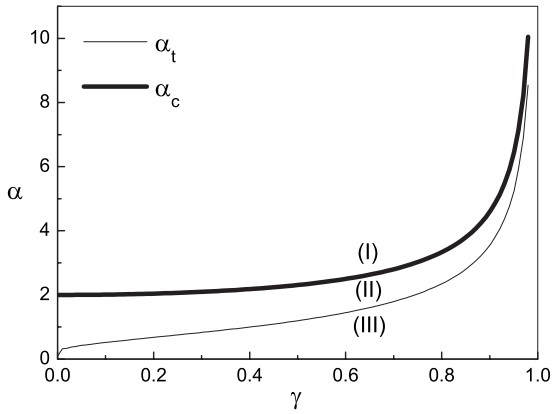

FIG. 4. Diagram $\alpha\times\gamma$ separating the distinct behaviors of $C(\alpha,\gamma,T)$ shown in Fig. 3. Regions (I), (II), and (III) correspond to the graphs shown in Figs. 3(a), 3(b), and 3(c), respectively. The curve $\alpha_c(\gamma)$ represents a regime of its own that is different from (I) and (II) [see Fig. 3(a)].

Figure 4 shows a diagram on the plane (α,γ) with regions corresponding to the different entanglement regimes. Note that for $\gamma=0$ we have $\alpha_t=0$, and therefore there are only two regions: (I) and (II). For $\gamma=1$, $\alpha_c\to\infty$ and $\alpha_t\to\infty$, and therefore there is just the regime (III). These two limiting cases were analyzed in Ref. [21]. These results imply that in the Ising model, only the parallel entanglement exists, while in the XX model, the antiparallel entanglement dominates. The curve $\alpha_c(\gamma)$ defines the lower limit of a region where the entanglement is described only by C_4, while the curve $\alpha_t(\gamma)$ sets the upper limit of a region where the entanglement is described by C_2. In the intermediate regime both types of behavior appear, creating the entanglement dip discussed previously. We can also use the boundary curves of Fig. 4 to obtain numerically an expression to the ratio α_t/α_c as a function of γ. We find the following linear relation:

$$\frac{\alpha_t(\gamma)}{\alpha_c(\gamma)} \simeq A + B\gamma, \tag{11}$$

where $A=0.193\pm0.002$ and $B=0.648\pm0.004$.

Preparing the ground for our discussion in Sec. IV concerning the characterization of entanglement patterns, we analyze the behavior of the probabilities of Bell states. Following Ref. [31] let $q_1(q_2)$ be the maximum probability for the occurrence of a (an) parallel (antiparallel) Bell state. The functions C_2 and C_4 can be written in terms of these probabilities [31] as $C_2=q_1-1/2$ and $C_4=q_2-(1-\Delta^2)/2$, where $\Delta^2=(\sqrt{q_{00}}-\sqrt{q_{11}})^2$, with q_{00} and q_{11} being the probabilities of the occurrence of the states $|00\rangle$ and $|11\rangle$, respectively. Note that $C=C_2$ if $q_1>1/2>q_2$, implying a connection between the entanglement and the predominance of a parallel state over the antiparallel ones. This justifies the term parallel entanglement in this case. In our model this characterization works well for $\alpha<\alpha_t$, where parallel entanglement is obtained. Similarly, we characterize the entanglement as antiparallel if $C=C_4$ and $q_2>q_1$. In our model this condition is

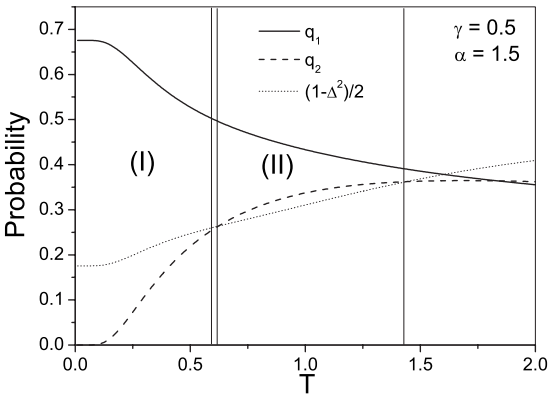

FIG. 5. Behavior of the probabilities q_1 and q_2 in the intermediate region $\alpha_t < \alpha < \alpha_c$. The vertical lines define four regions. In the regions denoted (I) and (II) the concurrence is positive, while it vanishes in the other two regions. In region (I), $q_1 > 1/2$ and the entanglement can be classified as parallel $C = C_2$. In region (II), although $q_1 > q_2$ the entanglement cannot be characterized as parallel because $C_2 < 0$ and $C = C_4$.

satisfied for $\alpha > \alpha_c$. Note however that it is not necessary to have $q_2 > q_1$ for $C = C_4$ if $\Delta \neq 0$ and therefore the characterization of antiparallel entanglement is more subtle than the parallel one. In Fig. 5 we show the behaviors of q_1 and q_2 in the intermediate region $\alpha_t < \alpha < \alpha_c$ as a function of the temperature. There are two different regions, denoted (I) and (II) in Fig. 5, where the concurrence is positive and two regions where the concurrence vanishes. In region (I) we have $C = C_2$, while $C = C_4$ in region (II). In both regions we have $q_1 > q_2$, which implies the predominance of a parallel Bell state over the antiparallel ones. Although the entanglement can be characterized as parallel in region (I), it cannot be classified as antiparallel in region (II). A similar conclusion was put forward in Ref. [32] regarding the characterization of finite temperature entanglement. The difficulty is due to the combined effects of temperature dependence of q_1 and q_2 and the presence of a magnetic field, which acts only on the parallel sector of the density matrix. If $h = 0 (\alpha \to \infty)$, $\Delta = 0$ and thus the predominance of one type of Bell state over the others becomes a sufficient condition for entanglement characterization at all temperatures. The difficulty also disappears at zero temperature.

Next, we study the behavior of the concurrence as a function of the parameter α maintaining γ and T fixed. This corresponds to performing cuts in Fig. 1 for different values of γ. In the upper part of Fig. 6, we present a diagram $\gamma \times T$ which exhibits a boundary curve separating two different regimes, denoted (I) and (II), which are characterized by the graphs shown in the lower part of the figure. A notable feature of region (I) is the presence of the entanglement dip on a finite interval of the domain of the parameter α. This feature is clearly absent in region (II).

Lastly, we analyze the dependence of $C(\alpha, \gamma, T)$ as a function of the anisotropy parameter γ keeping α and T fixed. The results are presented in the diagram shown in Fig. 7, which exhibits four different regions. In region (I) we have

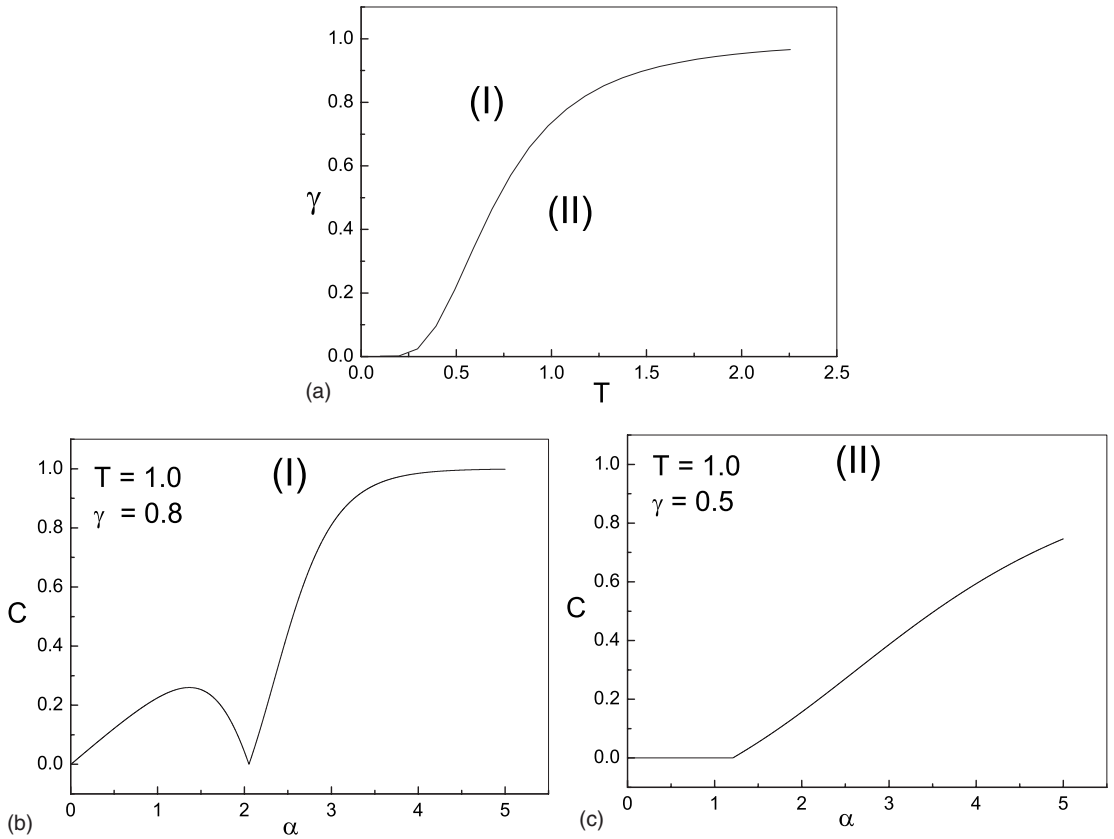

FIG. 6. Upper part: diagram $\gamma \times T$ separating different behaviors of $C(\alpha, \gamma, T)$ for fixed T and γ. Lower part: representative graphs of regions (I) and (II) of the above diagram.

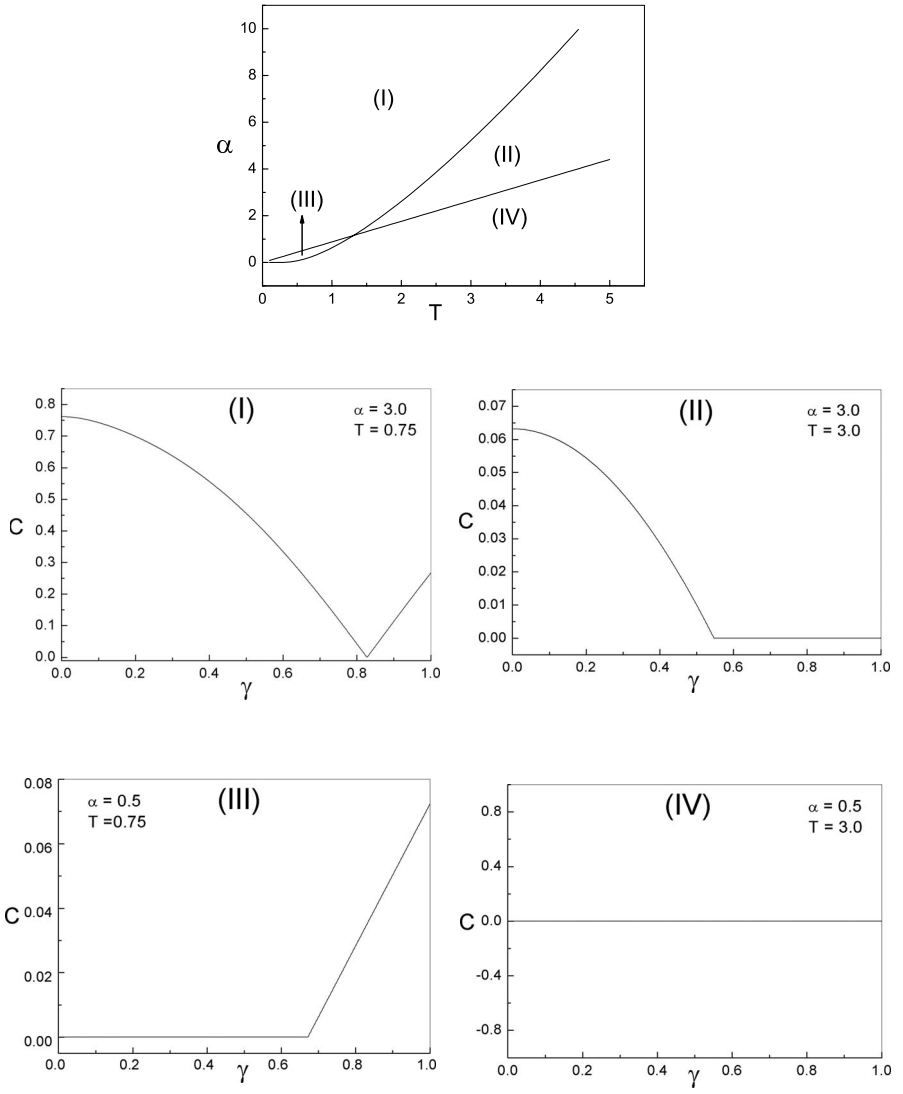

FIG. 7. Upper part: diagram $\alpha \times T$ showing the boundary lines separating four different regions. Lower part: behavior of $C(\alpha, \gamma, T)$, for T and α fixed, characterizing each region shown in the diagram above.

null concurrence in a small interval of values of γ, which corresponds to the values of α and γ for which $T > T_c(\alpha, \gamma)$. In region (II), the concurrence vanishes for values of γ above a certain threshold. The opposite occurs in region (III). The last region, (IV), corresponds to points (α, T) for which we have $T > T_c$ for all values of γ and therefore $C=0$ everywhere. A notable feature of the diagram is the existence of a crossing point of boundary curves, approximately at $T \approx 1.310$ and $\alpha = 1.155$. If we maintain one of the parameters T or α fixed at one of these values and let the other vary, we detected only two different entanglement patterns.

In Sec. IV, we shall demonstrate how these different classes of behavior of the concurrence function $C(\alpha, \gamma, T)$ or entanglement patterns translates into specific features of a pure quantum component of the spin-spin-correlation function.

IV. PURE QUANTUM CORRELATIONS

In Sec. III we demonstrated how the behavior of the concurrence function $C(\alpha, \gamma, T)$ can be used to separate regions in parameter space which exhibit different types of entanglement. In this section, we further characterize these entanglement patterns using suitably defined spin-correlation functions. We shall consider two types of correlation functions: (i) the usual ones which are obtained by thermal ensemble averages and (ii) the correlation functions defined via a mixture of states belonging to a special decomposition of the density matrix. This special decomposition appears in the calculation of the entanglement of formation [8] and has the property of minimizing the average concurrence. Ensemble averaged correlation functions are invariant under changes in density-matrix decompositions, which physically means that they quantify jointly both classical and quantum correlations. Therefore some properties of the thermal entangled state, which are revealed by the concurrence, may not be detected by these functions. The spin-correlation functions defined via the concurrence-minimizing decomposition, on the other hand, are sensitive to all features characterizing the different types of entanglement that occur in the system. In this section, we obtain explicitly the concurrence-minimizing decomposition, and using it we calculate the pure quantum

spin-correlation functions. Several graphs of these correlation functions are presented and compared with the correlation functions obtained by ensemble averages.

A. Concurrence-minimizing decomposition

It is known that any legitimate decomposition of the density matrix can be obtained as follows [2]: (i) find a legitimate decomposition $\{|v_i\rangle\}$ of the density matrix, ρ, and subnormalize the states of this decomposition in such a way that $\langle v_i|v_i\rangle=p_i$, where p_i is the probability of occurrence of the state $|v_i\rangle$ in the ensemble. In that way, ρ can be written as $\rho=\Sigma_{i=1}^{n}|v_i\rangle\langle v_i|$, where n is the rank of the density matrix; (ii) any legitimate decomposition of ρ can be obtained from $\{|v_i\rangle\}$ by using a higher dimensional unitary matrix. More specifically, if $|w_i\rangle$ is a legitimate decomposition of the density matrix, then there exists an $m\times m$ unitary matrix U, with $m\geq n$, such that $|w_i\rangle=\Sigma_{j=1}^{n}U_{ij}|v_j\rangle$.

Following Wooters' prescription [9], in order to obtain a concurrence-minimizing decomposition we need first to construct a legitimate decomposition, $\{|x_i\rangle\}$, of the density matrix with the special property $\langle x_i|\tilde{x}_j\rangle=\lambda_i\delta_{ij}$, where $|\tilde{x}_j\rangle$ is a "spin-flipped" state. From the considerations of the previous paragraph if we take the n subnormalized eigenstates of the density matrix as our initial decomposition than there exists an $m\times m$ unitary matrix U that acting on it produces the required decomposition $\{|x_i\rangle\}$. On the other hand, one can show that the states $\{|x_i\rangle\}$ are in fact right eigenstates of the non-Hermitian matrix $R=\rho\tilde{\rho}=\rho\sigma^y\otimes\sigma^y\rho^*\sigma^y\otimes\sigma^y$, so that the desired decomposition can also be obtained by normalizing the right eigenstates of R in such a way that the required property is satisfied. We applied both procedures and verified that they lead to the same decomposition, which was taken as a consistency check. The final results are

$$|x_1\rangle=\sqrt{\frac{\lambda_1}{2}}\left[\left(\frac{p}{r}\right)^{1/4}|00\rangle-\left(\frac{r}{p}\right)^{1/4}|11\rangle\right], \tag{12}$$

$$|x_2\rangle=-i\sqrt{\frac{\lambda_2}{2}}\left[\left(\frac{p}{r}\right)^{1/4}|00\rangle+\left(\frac{r}{p}\right)^{1/4}|11\rangle\right], \tag{13}$$

$$|x_3\rangle=-i\sqrt{\frac{\lambda_3}{2}}[|01\rangle-|10\rangle], \tag{14}$$

$$|x_4\rangle=\sqrt{\frac{\lambda_4}{2}}[|01\rangle+|10\rangle]. \tag{15}$$

The next step is to find a unitary transformation that maps the decomposition $\{|x_i\rangle\}$ onto a new one $\{|z_i\rangle\}$ with the property that it minimizes the average concurrence. It can be shown [9,33] that this result can be easily obtained from the following representation:

$$|z_1\rangle=\tfrac{1}{2}[|y_1\rangle+e^{i\theta_2}|y_2\rangle+e^{i\theta_3}|y_3\rangle+e^{i\theta_4}|y_4\rangle], \tag{16}$$

$$|z_2\rangle=\tfrac{1}{2}[|y_1\rangle+e^{i\theta_2}|y_2\rangle-e^{i\theta_3}|y_3\rangle-e^{i\theta_4}|y_4\rangle], \tag{17}$$

$$|z_3\rangle=\tfrac{1}{2}[|y_1\rangle-e^{i\theta_2}|y_2\rangle+e^{i\theta_3}|y_3\rangle-e^{i\theta_4}|y_4\rangle], \tag{18}$$

$$|z_4\rangle=\tfrac{1}{2}[|y_1\rangle-e^{i\theta_2}|y_2\rangle-e^{i\theta_3}|y_3\rangle+e^{i\theta_4}|y_4\rangle], \tag{19}$$

where the states $\{|y_i\rangle\}$ correspond to the states $\{|x_j\rangle\}$ rearranged in such a way that $|y_1\rangle$ equals the state $|x_i\rangle$ for which $\lambda_i=\lambda^{\max}$. The average concurrence of that decomposition is given by $\langle C\rangle=\Lambda_1+\Sigma_{j>1}\Lambda_j e^{-2i\theta_j}$, where the set $\{\Lambda_j\}$ corresponds to the set $\{\lambda_i\}$ rearranged in decreasing order. In the regions where $2\lambda^{\max}-\Sigma_{j=1}^{4}\lambda_j>0$, the concurrence-minimizing decomposition is given by taking $\{|z_i\rangle\}$ with the choice $\theta_2=\theta_3=\theta_4=\pi/2$. There are two types of decompositions of the density matrix which refer to the conditions $\Lambda_1=\lambda_2$ and $\Lambda_1=\lambda_4$. These two decompositions have very different characteristics as were shown in Sec. IV through the behavior of the functions C_2 and C_4. Notice that the states $[|x_1\rangle,|x_2\rangle]$ belong to the parallel sector, while $[|x_3\rangle,|x_4\rangle]$ belong to the antiparallel one. However, to find the concurrence-minimizing decomposition we need to mix states from both sectors. This reveals the difficulty to interpret the functions C_2 and C_4 as parallel and antiparallel entanglements, as we have discussed in Sec. IV. We shall analyze these two decompositions separately.

Case 1: $\lambda_4>\lambda_2$. In this case we have $|y_1\rangle=|x_4\rangle$. The concurrence-minimizing decomposition, denoted $\{|w_i\rangle\}$, is given by

$$|w_1\rangle=\tfrac{1}{2}[|x_4\rangle+i|x_1\rangle+i|x_2\rangle+i|x_3\rangle], \tag{20}$$

$$|w_2\rangle=\tfrac{1}{2}[|x_4\rangle+i|x_1\rangle-i|x_2\rangle-i|x_3\rangle], \tag{21}$$

$$|w_3\rangle=\tfrac{1}{2}[|x_4\rangle-i|x_1\rangle+i|x_2\rangle-i|x_3\rangle], \tag{22}$$

$$|w_4\rangle=\tfrac{1}{2}[|x_4\rangle-i|x_1\rangle-i|x_2\rangle+i|x_3\rangle]. \tag{23}$$

All states of this decomposition have the same probability of occurrence $p=1/4$. The concurrence is thus the same for every state and this decomposition also minimizes the entanglement of formation.

Case 2: $\lambda_2>\lambda_4$. In this case we have $|y_1\rangle=|x_2\rangle$. From the general representation of the states $\{|z_i\rangle\}$ and the expression for $\{|x_i\rangle\}$ we obtain

$$|z_1\rangle=\tfrac{1}{2}[|x_2\rangle+i|x_1\rangle+i|x_3\rangle+i|x_4\rangle], \tag{24}$$

$$|z_2\rangle=\tfrac{1}{2}[|x_2\rangle+i|x_1\rangle-i|x_3\rangle-i|x_4\rangle], \tag{25}$$

$$|z_3\rangle=\tfrac{1}{2}[|x_2\rangle-i|x_1\rangle+i|x_3\rangle-i|x_4\rangle], \tag{26}$$

$$|z_4\rangle=\tfrac{1}{2}[|x_2\rangle-i|x_1\rangle-i|x_3\rangle+i|x_4\rangle]. \tag{27}$$

Unlike the previous case the states of this decomposition are not equally probable and consequently they do not have the same concurrence. Therefore, although this decomposition minimizes the average concurrence it does not minimize the entanglement of formation. However, we verified numerically that the discrepancy is very small so that it can still be used for practical purposes. The probabilities of occurrence of the states in the concurrence-minimizing decomposition are given by

$$p_1 = p_2 = \frac{1}{4}\left[1 - \frac{\mathcal{Q}}{Z}\right], \tag{28}$$

$$p_3 = p_4 = \frac{1}{4}\left[1 + \frac{\mathcal{Q}}{Z}\right], \tag{29}$$

where $z=2(\cosh\Delta+\cosh\Delta_c)$ is the partition function and

$$\mathcal{Q} = \frac{4}{\sqrt{4+\alpha^2\gamma^2}}\frac{\sinh\Delta_c}{\sqrt{1+q^2}}. \tag{30}$$

In the regions where $C(\rho)=0$, the phases θ_2, θ_3, and θ_4 are chosen such that $C=\lambda_1+\Sigma_{j>1}\lambda_j e^{-2i\theta_j}=0$. This choice is always possible when $\lambda_1<\lambda_2+\lambda_3+\lambda_4$. Making this choice, we obtain a decomposition corresponding to separable pure states. For these states, as we shall demonstrate, the pure quantum spin correlations vanish. This does not mean, however, that the ensemble averaged spin correlations should also vanish since the statistical mixture of these states allows for the existence of classical correlations. In fact, in these regions the correlations between the spins are purely classical in the sense of being generated solely by local operations and classical communications [2].

B. Spin correlation functions

In this section we present a detailed quantitative analysis of the properties of the spin-correlation functions of the system. We start by presenting exact expressions for the spin-correlation functions of the states in the concurrence-minimizing decomposition and also for ensemble averaged correlation functions. Comparative graphs will illustrate their differences and similarities. Spin correlation functions are defined as quantum averages,

$$\Gamma_{\alpha\beta} \equiv \langle\sigma_1^\alpha\sigma_2^\beta\rangle - \langle\sigma_1^\alpha\rangle\langle\sigma_2^\beta\rangle, \tag{31}$$

where $\alpha,\beta\in(x,y,z)$.

We show that the average correlation functions calculated on the states of the concurrence-minimizing decompositions correspond to a pure quantum component of the correlations.

For the decomposition $\{|z_i\rangle\}$, the correlation functions for the pure states $|z_1\rangle$ and $|z_2\rangle$ are the same and similarly for $|z_3\rangle$ and $|z_4\rangle$. We denote them as $\Gamma_{\alpha\beta}(z_{1,2})$ and $\Gamma_{\alpha\beta}(z_{3,4})$, respectively. The pure quantum spin-correlation function is then defined by the following weighted average:

$$\Gamma^q_{\alpha\beta} = 2p_1\Gamma_{\alpha\beta}(z_{1,2}) + 2p_3\Gamma_{\alpha\beta}(z_{3,4}), \tag{32}$$

where

$$\Gamma_{xx}(z_{1,2}) = \frac{2(q+\sinh\Delta)}{Z-\mathcal{Q}} - \frac{e^{\Delta}(4\cosh\Delta_c - 2\mathcal{Q}+4q)}{(Z-\mathcal{Q})^2}, \tag{33}$$

$$\Gamma_{yy}(z_{1,2}) = \frac{2(-q+\sinh\Delta)}{Z-\mathcal{Q}} + \frac{e^{-\Delta}(4\cosh\Delta_c - 2\mathcal{Q}+4q)}{(Z-\mathcal{Q})^2}, \tag{34}$$

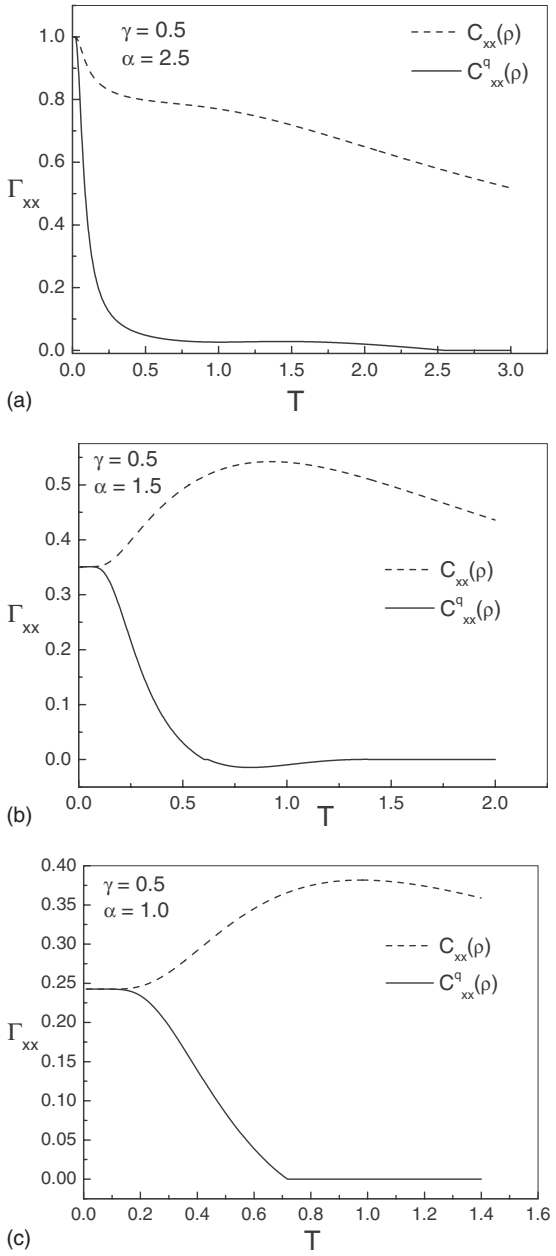

FIG. 8. Behavior of the spin-correlation functions as a function of temperature for each region in the diagram shown in Fig. 4. The full lines represent the pure quantum component Γ^q_{xx}, while the dashed lines represent the ensemble averaged spin-correlation function.

$$\Gamma_{zz}(z_{1,2}) = \frac{2\cosh\Delta_c - \mathcal{Q} - 2\cosh\Delta}{Z-\mathcal{Q}} - \frac{[(1+q^2)\mathcal{Q} - 2\cosh\Delta_c]^2}{(Z-\mathcal{Q})^2(1+q^2)}, \tag{35}$$

and

$$\Gamma_{xx}(z_{3,4}) = \frac{2(q+\sinh\Delta)}{Z+\mathcal{Q}} - \frac{e^{\Delta}(4\cosh\Delta_c + 2\mathcal{Q}+4q)}{(Z+\mathcal{Q})^2}, \tag{36}$$

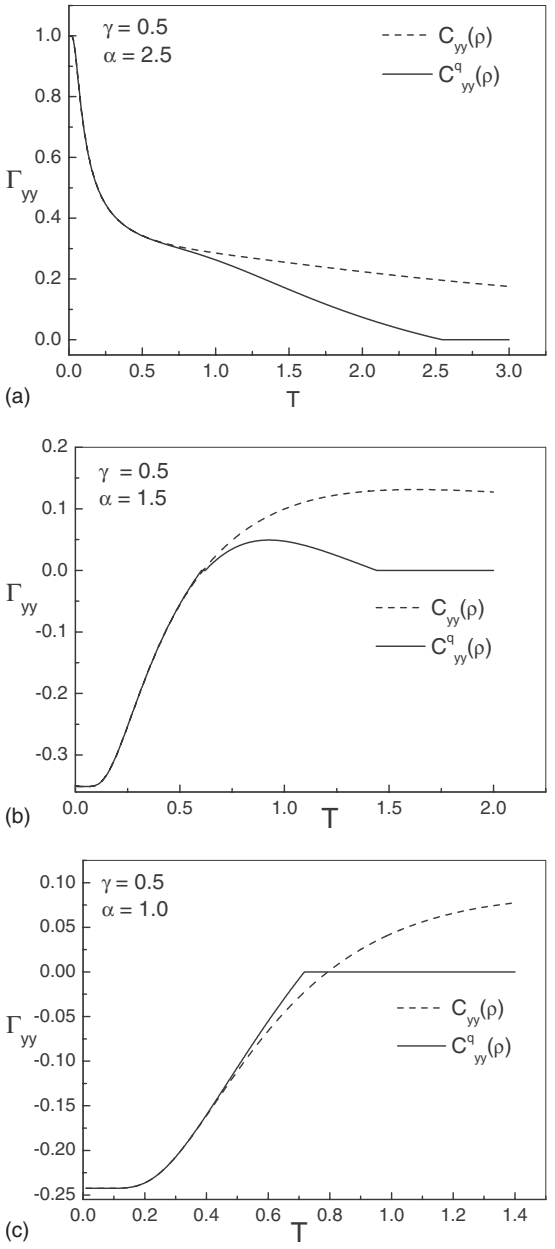

FIG. 9. Behavior of the spin-correlation functions as a function of temperature for each region in the diagram shown in Fig. 4. The full lines represent the pure quantum component Γ^q_{yy}, while the dashed lines represent the ensemble averaged spin-correlation function.

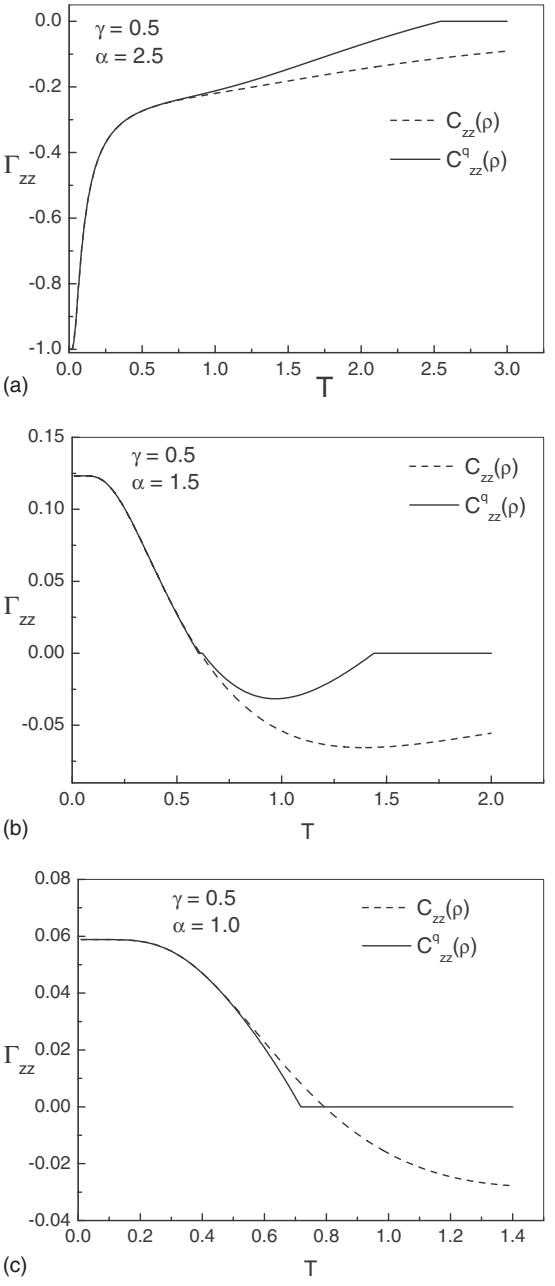

FIG. 10. Behavior of the spin-correlation functions as a function of temperature for each region in the diagram shown in Fig. 4. The full lines represent the pure quantum component Γ^q_{zz}, while the dashed lines represent the ensemble averaged spin-correlation function.

$$\Gamma_{yy}(z_{3,4}) = \frac{2(-q+\sinh\Delta)}{Z+\mathcal{Q}} + \frac{e^{-\Delta}(4\cosh\Delta_c + 2\mathcal{Q} + 4q)}{(Z+\mathcal{Q})^2}, \tag{37}$$

$$\Gamma_{zz}(z_{3,4}) = \frac{2\cosh\Delta_c + \mathcal{Q} - 2\cosh\Delta}{Z+\mathcal{Q}} - \frac{[(1+q^2)\mathcal{Q} + 2\cosh\Delta_c]^2}{(Z+\mathcal{Q})^2(1+q^2)}. \tag{38}$$

For the decomposition $\{|w_i\rangle\}$, the correlation functions are the same for all the states. We find

$$\Gamma_{xx}(w_{1-4}) = \frac{2(q+\sinh\Delta)}{Z} - \frac{4(\sqrt{1+q^2}+q)[\mathcal{P}\sinh\Delta + \cosh\Delta]}{Z^2},$$

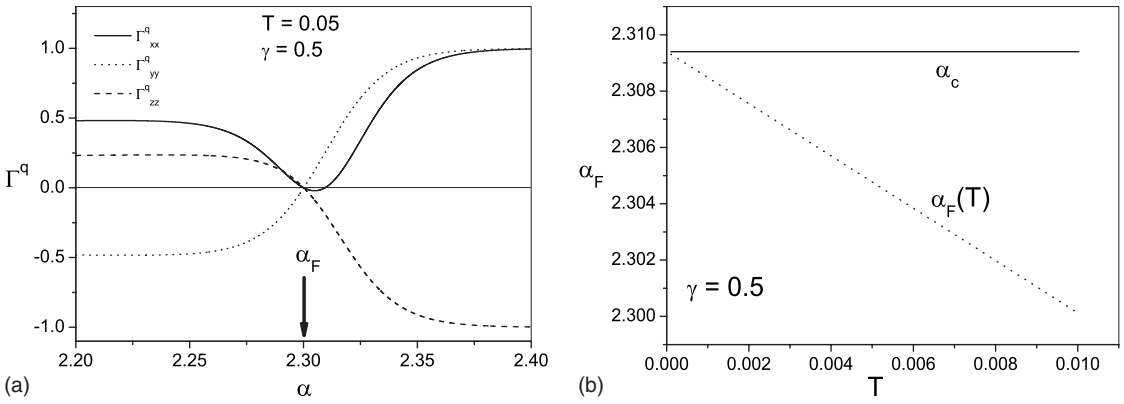

FIG. 11. (a) Pure quantum correlation functions in the neighborhood of the factorizing field α_f at which they all vanish; (b) factorizing field as a function of temperature. Note that $\alpha_f \to \alpha_c$ when $T \to 0$.

$$\Gamma_{yy}(w_{1-4}) = \frac{2(-q+\sinh\Delta)}{Z} - \frac{4(\sqrt{1+q^2}-q)[\mathcal{P}\sinh\Delta+\cosh\Delta]}{Z^2},$$

$$\Gamma_{zz}(w_{1-4}) = \frac{2(\cosh\Delta_c-\cosh\Delta)}{Z} - \frac{[\mathcal{Q}^2(1+q^2)-4]}{Z^2},$$

where $\mathcal{P}=\cosh\Delta_c/\sqrt{1+q^2}$. In this case the pure quantum correlation function is simply $\Gamma^q_{\alpha\beta}=\Gamma_{\alpha\beta}(w_{1-4})$. In summary, the formula

$$\Gamma^q_{\alpha\beta} = \begin{cases} \Gamma_{\alpha\beta}(w_{1-4}), & \lambda_4 > \lambda_2 \\ 2p_1\Gamma_{\alpha\beta}(z_{1-2}) + 2p_3\Gamma_{\alpha\beta}(z_{3-4}), & \lambda_2 > \lambda_4 \end{cases}$$

can be used as an operational definition of the pure quantum spin-correlation function of the system.

The pure quantum spin-correlation functions calculated previously vanish, by construction, when the states are separable. However, the full density matrix of the system is a statistical mixture of these states that leads to decomposition invariant averages, which implies that it must also include some degree of classical correlations. Therefore, the ensemble averaged correlation functions do not vanish if we choose a decomposition containing only separable states. These correlation functions are defined as

$$\Gamma_{\alpha\beta}(\rho) \equiv \mathrm{Tr}[\sigma_1^\alpha\sigma_2^\beta\rho] - \mathrm{Tr}[\sigma_1^\alpha\rho]\mathrm{Tr}[\sigma_2^\beta\rho] = \sum_{j=1}^{4}\langle\Psi_j|\sigma_1^\alpha\sigma_2^\beta|\Psi_j\rangle - \sum_{j=1}^{4}\langle\Psi_j|\sigma_1^\alpha|\Psi_j\rangle\sum_{k=1}^{4}\langle\Psi_k|\sigma_2^\beta|\Psi_k\rangle, \quad (39)$$

where $\{|\Psi_j\rangle\}$ is an arbitrary decomposition of the density matrix. Notice that these correlation functions do not depend on the decomposition since they can be written directly in terms of the density matrix. Applying this definition to our problem, we obtain the following results:

$$\Gamma_{xx}(\rho) = \frac{2(q+\sinh\Delta)}{Z}, \quad (40)$$

$$\Gamma_{yy}(\rho) = \frac{2(-q+\sinh\Delta)}{Z}, \quad (41)$$

$$\Gamma_{zz}(\rho) = \frac{2(\cosh\Delta_c-\cosh\Delta)}{Z} - (1+q^2)\left(\frac{\mathcal{Q}}{Z}\right)^2. \quad (42)$$

Since these correlation functions quantify jointly classical and quantum correlations, they are not sensitive to the entanglement patterns described in Sec. III.

We proceed by presenting some graphs of the correlation functions as a function of the temperature for several values of the system's parameters α and γ. We find that the pure quantum correlation functions are strongly sensitive to parameter variations that lead to changes in the entanglement patterns, whose boundaries are defined by the curves $\alpha_c(\gamma)$ and $\alpha_t(\gamma)$. Figure 8 shows the behavior of Γ_{xx} as a function of the temperature for $\gamma=0.5$ and three different values of α representing the three regions shown in the diagram of Fig. 4.

The behaviors of Γ_{yy} and Γ_{zz} are somewhat less dramatic, but they also show clear signatures distinguishing the regions associated with different entanglement patterns. They are shown in Figs. 9 and 10, respectively. Note in particular that the ensemble averaged correlation functions completely miss the entanglement features related to the existence of the boundary line $\alpha_t(\gamma)$ shown in the diagram of Fig. 4.

We close this section by showing an interesting connection with the theory of classical-like ground states (CGSs) [34]. It states that pure quantum fluctuations may vanish at certain values of the control parameters and the ground state of the quantum system becomes identical to the lowest-energy state of its classical counterpart. Extending this idea to low-temperature thermal states, we have verified the existence of a factorizing field α_f, at which the concurrence and all pure quantum correlation functions vanish. This point approaches the value α_c when $T \to 0$ as shown in Fig. 11.

V. SUMMARY AND CONCLUSIONS

In this paper we investigated the possibility of the existence of different types of thermal entanglement in the two-spin Heisenberg XY model. Our main motivation was the

connection, valid in the thermodynamic limit, between quantum order on one hand and entanglement patterns on the other [28,29]. We were also guided by the possibility of using the concept of entanglement as a generalized notion of order with features that could also be manifested in clusters of coupled qubits [7]. A particular intriguing aspect of thermal entanglement in clusters of qubits is the existence of a temperature threshold above which the entanglement vanishes [26]. Combining singular features of the temperature threshold of the two-spin Heisenberg *XY* model with ground-state discontinuities as a function of the model parameters, we could identify classes of behaviors of the concurrence that led to a quantitative characterization of entanglement patterns in the system, which were shown in diagrams. These different types of entanglement were further characterized by an operationally defined procedure to extract a pure quantum component of the ensemble averaged spin-correlation function. These pure quantum spin-correlation functions were shown to be highly sensitive to changes in the classes of entanglement types and were also shown to vanish for separable states.

We believe that the concepts discussed in this work may bring insights in the development of entanglement as a powerful concept to unify theoretical tools in condensed-matter systems. We are particularly interested in applying the concepts developed here to the theory of full counting statistics of charge transfer through interacting mesoscopic systems [35], where qubits can be used as a measurement device. We are specially intrigued by the possibility that entanglement patterns could play a role in the design of highly efficient and selective detectors. Another interesting challenge for research in the immediate future is the construction of entanglement witnesses that are sensitive to changes in entanglement patterns.

ACKNOWLEDGMENTS

This work was partially supported by CNPq and FACEPE (Brazilian Agencies).

[1] C. H. Bennett and D. P. DiVincenzo, Nature (London) **404**, 247 (2000).
[2] M. A. Nielsen and I. L. Chuang, *Quantum Computation and Quantum Information* (Cambridge University Press, Cambridge, 2000).
[3] For a recent review, see R. Horodecki, P. Horodecki, M. Horodecki, and K. Horodecki, e-print arXiv:quant-ph/0702225.
[4] S. Sachdev, *Quantum Phase Transitions* (Cambridge University Press, Cambridge, 2000).
[5] L. Amico, R. Fazio, A. Osterloh, and V. Vedral, Rev. Mod. Phys. **80**, 517 (2008).
[6] A. Anfossi, P. Giorda, and A. Montorsi, Phys. Rev. B **75**, 165106 (2007).
[7] J. Anders and V. Vedral, Open Syst. Inf. Dyn. **14**, 1 (2007).
[8] C. H. Bennett, D. P. DiVincenzo, J. A. Smolin, and W. K. Wootters, Phys. Rev. A **54**, 3824 (1996).
[9] W. K. Wootters, Phys. Rev. Lett. **80**, 2245 (1998).
[10] F. Mintert, M. Kuś, and A. Buchleitner, Phys. Rev. Lett. **92**, 167902 (2004).
[11] G. Vidal and R. F. Werner, Phys Rev. A **65**, 032314 (2002).
[12] J. Kempe, Contemp. Phys. **44**, 307 (2003).
[13] A. P. Hines and P. C. E. Stamp, Phys. Rev. A **75**, 062321 (2007).
[14] G. Vidal, J. I. Latorre, E. Rico, and A. Kitaev, Phys. Rev. Lett. **90**, 227902 (2003).
[15] J. I. Latorre, R. Rico, and G. Vidal, Quantum Inf. Comput. **4**, 48 (2004).
[16] B.-Q. Jin and V. E. Korepin, J. Stat. Phys. **116**, 79 (2004).
[17] J. P. Keating and F. Mezzadri, Commun. Math. Phys. **252**, 543 (2004).
[18] M. A. Nielsen, Ph.D. thesis, University of New Mexico, New Mexico, 1998; arXiv:quant-ph/0011036v1.
[19] G. L. Kamta and A. F. Starace, Phys. Rev. Lett. **88**, 107901 (2002).
[20] C. Anteneodo and A. M. C. Souza, J. Opt. B: Quantum Semiclassical Opt. **5**, 73 (2003).
[21] X. Wang, Phys. Rev. A **64**, 012313 (2001).
[22] T. J. Osborne and M. A. Nielsen, Phys. Rev. A **66**, 032110 (2002).
[23] M. C. Arnesen, S. Bose, and V. Vedral, Phys. Rev. Lett. **87**, 017901 (2001).
[24] S.-J. Gu, H. Li, Y.-Q. Li, and H.-Q. Lin, Phys. Rev. A **70**, 052302 (2004).
[25] Z. Xiao-Yue and T. Pei-Qing, Chin. Phys. Lett. **24**, 2475 (2007).
[26] B. V. Fine, F. Mintert, and A. Buchleitner, Phys. Rev. B **71**, 153105 (2005).
[27] A. Osterloh, L. Amico, G. Falci, and R. Fazio, Nature (London) **416**, 608 (2002).
[28] X.-G. Wen, *Quantum Field Theory of Many-Body Systems* (Oxford University Press, Oxford, UK, 2004).
[29] X.-G. Wen, Phys. Rev. Lett. **90**, 016803 (2003).
[30] I. Žutić, J. Fabian, and S. Das Sarma, Rev. Mod. Phys. **76**, 323 (2004).
[31] A. Fubini, T. Roscilde, V. Tognetti, M. Tusa, and P. Verruchi, Eur. Phys. J. D **38**, 563 (2006).
[32] L. Amico, F. Baroni, A. Fubini, D. Patane, V. Tognetti, and P. Verrucchi, Phys. Rev. A **74**, 022322 (2006).
[33] F. Mintert, Ph.D. thesis, Ludwig-Maximilians Universität München, München, 2004 (http://edoc.ub.uni-muenchen.de/archive/00002133).
[34] J. Kurmann, H. Thomas, and G. Müller, Physica A **112**, 235 (1982).
[35] A. M. S. Macêdo, Phys. Rev. B **69**, 155309 (2004).